# Three-Dimensional Solution Structure of a Curaremimetic Toxin from *Naja nigricollis* Venom: A Proton NMR and Molecular Modeling Study

Sophie Zinn-Justin, Christian Roumestand, Bernard Gilquin, François Bontems, André Ménez, and Flavio Toma*

*Laboratoire de Structure des Protéines en Solution, Département d'Ingénierie et d'Etude des Protéines, CE-Saclay, 91191 Gif-sur-Yvette Cedex, France*

*Received June 8, 1992; Revised Manuscript Received August 21, 1992*

ABSTRACT: The solution conformation of toxin α from *Naja nigricollis* (61 amino acids and four disulfides), a snake toxin which specifically blocks the activity of the nicotinic acetylcholine receptor (AcChoR), has been determined using nuclear magnetic resonance spectroscopy and molecular modeling. The solution structures were calculated using 409 distance and 73 dihedral angle restraints. The average atomic rms deviation between the eight refined structures and the mean structure is ~0.5 Å for the backbone atoms. The overall folding of toxin α consists of three major loops which are stabilized by three disulfide bridges and one short C terminal loop stabilized by a fourth disulfide bridge. All the disulfides are grouped in the same region of the molecule, forming a highly constrained structure from which the loops protude. As predicted, this structure appears to be very similar to the 1.4-Å resolution crystal structure of another snake neurotoxin, namely, erabutoxin b from *Laticauda semifasciata*. The atomic rms deviation for the backbone atoms between the solution and crystal structures is ~1.7 Å. The minor differences which are observed between the two structures are partly related to the deletion of one residue from the chain of toxin α. It is notable that, although the two toxins differ from each other by 16 amino acid substitutions, their side chains have an essentially similar spatial organization. However, most of the side chains which constitute the presumed AcChoR binding site for the curaremimetic toxins are poorly resolved in toxin α. These side chains are solvent exposed, and their conformation in the crystal structure of erabutoxin b is only one of the conformations which exist in the solution structures of toxin α.

Venoms from elapid and hydrophid snakes are complex mixtures of proteins among which some are potent toxins. These toxins selectively perturb essential physiological systems of snake preys mostly by targetting ion channels, receptors, and enzymes.

Toxin α from *Naja nigricollis* (61 amino acids and four disulfides) is the first curaremimetic toxin whose complete amino acid sequence has been reported (Eaker & Porath, 1967). It binds to nicotinic acetylcholine receptors with specificity and high affinity ($K_d$ = 5 × $10^{-11}$ M), thus maintaining the channel in a closed and resting state (Popot & Changeux, 1984). Tritium-labeled toxin α has played an important role in the isolation and characterization of AcChoR[1] from *Electrophorus electricus* (Meunier et al., 1972) and *Torpedo marmorata* (Weber & Changeux, 1974). Toxin α has subsequently been subjected to several studies aiming at mapping the sites that are recognized by AcChoR (Faure et al., 1983) or neutralizing monoclonal antibodies [reviewed in Ménez et al. (1991)]. Strikingly, however, the three-dimensional structure of toxin α remained unknown.

Other snake toxins with similar curaremimetic activity have been isolated and characterized. On the basis of various considerations including circular dichroism studies and prediction analysis of secondary structure, common structural features have been suggested for these toxins (Dufton & Hider, 1977, 1988; Ménez et al., 1978; Karlsson et al., 1979; Endo & Tamiya, 1987). Thus it was anticipated that the overall folding of the polypeptide chain of toxin α is similar to that of other curaremimetic toxins, as elucidated by X-ray crystallography (Low et al., 1976; Tsernoglou & Petsko, 1976; Smith et al., 1988; Corfield et al., 1989; Agard & Stroud, 1982; Love & Stroud, 1986; Walkinshaw et al., 1980; Betzel et al., 1991) or NMR spectroscopy (Labhardt et al., 1988; Yu et al., 1990; Inagaki et al., 1985; Basus et al., 1988; Laplante et al., 1990; Le Goas et al., 1992). More precisely, it was usually assumed that the three-dimensional structure of toxin α closely resembles that of erabutoxin a (Corfield et al., 1989) and erabutoxin b from *Laticauda semifasciata* (Low et al., 1976; Tsernoglou & Petsko, 1976; Smith et al., 1988), which differ from toxin α by 16 amino acid residues and one insertion at position 18.

In the present paper, we report the detailed solution structure of toxin α, as deduced from 2D NMR spectroscopy and molecular modeling. The structure is compared with that of erabutoxin b. In addition, the conformation of the side chains that form the presumed receptor binding site is analyzed in detail for both toxin α and erabutoxin b.

## MATERIAL AND METHODS

*Sample Preparation.* Toxin α was purified from *N. nigricollis* venom (Institut Pasteur, Paris, France) as described previously (Fryklund & Eaker, 1975). For the NMR measurements, about 10 mg of toxin was dissolved in 0.4 mL of solvent, so that the final concentration was 4 mM. The solvents used were either a mixture of 95% (v/v) $H_2O$ and 5% (v/v) $D_2O$ at pH 3.5 or 100% $D_2O$ at pD 3.5. The pH (pD) was adjusted by the addition of microliter amounts of dilute HCl (DCl). For the preparation of samples in $D_2O$, the amide protons were previously fully exchanged with deuterium by keeping the solution at 50 °C for 5 h. Chemical shifts were

* To whom correspondence should be addressed.

[1] Abbreviations: AcChoR, acetylcholine nicotinic receptor; NMR, nuclear magnetic resonance; 2D, two dimensional; COSY, correlated spectroscopy; 2Q-COSY, double-quantum correlated spectroscopy; 2QF-COSY, double-quantum filtered correlated spectroscopy; TOCSY, total correlated spectroscopy; NOE, nuclear Overhauser effect; NOESY, NOE spectroscopy; AMX, spin system of three different protons; rmsd, root mean square deviation.

0006-2960/92/0431-11335$03.00/0 

Table I: Protocol Used for the Simulated Annealing Calculations

during phases 1–4
force field: parmallhSA
time step = 0.5 fs
$K$(bond) = 600 kcal·mol$^{-1}$·Å$^{-2}$, except in phase 4
$K$(angle) = 500 kcal·mol$^{-1}$·rad$^{-2}$, except in phase 4
$K$(dihe) = 500 kcal·mol$^{-1}$·rad$^{-2}$, when corresponding to planarity of peptide groups and aromatic rings, else $K$(dihe) = 0

phase 1: minimization
$K$(NOE) = 0 kcal·mol$^{-1}$·Å$^{-2}$
$K$(Cdihe) = 0 kcal·mol$^{-1}$·rad$^{-2}$
$K$(repel) = 0.01 kcal·mol$^{-1}$·Å$^{-4}$

phase 2: thermalization and introduction of NMR restraints, 20 cycles of 200 steps
temperature = 0 → 1000 K
$K$(NOE) = 0.1 → 50 kcal·mol$^{-1}$·Å$^{-2}$
$K$(Cdihe) = 0.1 → 20 kcal·mol$^{-1}$·rad$^{-2}$
$K$(repel) = 0.01 kcal·mol$^{-1}$·Å$^{-4}$
disulfide bridges:
$K_b$(S–S) = 0.1 → 500 kcal·mol$^{-1}$·Å$^{-2}$
$K_a$(C–S–S) = 0.1 → 500 kcal·mol$^{-1}$·rad$^{-2}$
$K_d$(C–S–S–C) = 0.1 → 2 kcal·mol$^{-1}$·rad$^{-2}$

phase 3: 8000 steps of equilibration; increase of the repulsive function: 10 cycles of 500 steps
$K$(repel) = 0.01 → 4 kcal·mol$^{-1}$·Å$^{-4}$, 8000 steps of equilibration

phase 4: decrease of the temperature, 80 cycles of 100 steps
temperature = 1000 → 0K
$K$(bond) = 600 → 400 kcal·mol$^{-1}$·Å$^{-2}$
$K$(angle) = 500 → 40 kcal·mol$^{-1}$·rad$^{-2}$
disulfide bridges:
$K_b$(S–S) = 500 → 400 kcal·mol$^{-1}$·Å$^{-2}$
$K_a$(C–S–S) = 500 → 40 kcal·mol$^{-1}$·rad$^{-2}$

phase 5: 1000 steps of restrained molecular dynamics at 0 K
time step = 1 fs
force field: parmallh3x, derived from CHARMM param19 file (Brooks et al., 1983)
$K$(NOE) = 25 kcal·mol$^{-1}$·Å$^{-2}$
$K$(Cdihe) = 20 kcal·mol$^{-1}$·rad$^{-2}$

measured relative to 3-trimethylsilyl-[2,2,3,3-$^2H_4$]propionate used as internal reference.

*NMR Spectroscopy.* Proton 2D NMR experiments, namely, COSY (Aue et al., 1976), 2QF-COSY (Rance et al., 1983), 2Q-COSY (Wagner & Zuiderweg, 1983), TOCSY (Davis & Bax, 1985), and NOESY (Kumar et al., 1980), were carried out either at 500 MHz on a Bruker AMX500 spectrometer or at 600 MHz on a Bruker AMX600 spectrometer. Complete signal assignment was achieved by recording spectra at different temperatures (293, 298, 303, 308, and 318 K). TOCSY spectra were recorded with an 80-ms isotropic mixing period. A WALTZ 16 composite pulse was used for the isotropic mixing, and a pair of $Z$-filters with a delay of 3 μs were inserted on either end of the spin-lock pulse to overcome phase anomalies. NOESY spectra were recorded with mixing times of 100, 150, and 300 ms in $H_2O$ and a mixing time of 300 ms in $D_2O$.

The experiments were performed using the time-proportional phase incrementation method (Bodenhausen et al., 1984) in the $t_1$ dimension and were collected in simultaneous acquisition mode in the $t_2$ dimension. The water signal was suppressed by low-power irradiation of the solvent resonance at all times except during $t_1$ and $t_2$.

The spectra were recorded with 512 ($t_1$) × 2048 ($t_2$) data points (1024 × 4096 for 2Q and 2QF-COSY) and with a spectral width of 7812 Hz at 600 MHz. All experiments were zero-filled in the $t_1$ dimension in order to achieve the same resolution in each dimension. They were multiplied by a phase-shifted sine bell function in both dimensions prior to Fourier transformation. Data processing was carried out with the NMRI program on a SUN Sparc station 1.

NH–C$^\alpha$H and C$^\alpha$H–C$^\beta$H coupling constants were determined from the high-resolution COSY spectra by measuring the peak-to-peak distances on a cross section parallel to the $\omega_2$ axis. In these experiments, the digital resolution after zero-filling along $\omega_2$ was 0.5 Hz.

Proton–deuterium exchange of the amide groups was studied on a sample of toxin α lyophilized from $H_2O$ and redissolved in pure $D_2O$. The residual NH signal was followed with time at 298 K by absolute value COSY experiments consisting of 256 FIDs of eight scans, each scan being composed of 1024 time-domain data points. Each experiment was completed in 25 min. Spectra were recorded every 30 min during 48 h. Exchange rates were determined by the least-squares fit of a single-exponential decay using the peak volume of nonoverlapping COSY cross-peaks.

*Experimental Restraints.* The intensities of the NOEs were measured on spectra recorded with a mixing time of 150 ms. To relate these NOE data with intramolecular interproton distances, a distance calibration was made using the standard distance of 2.2 Å for the interresidue (C$^\alpha$H, NH) sequential effect in β-strands. Intraresidue and sequential NOEs were divided into three groups, strong, medium, and weak NOEs, corresponding to upper bounds of 2.5, 3.5, and 4.5 Å respectively. For backbone–backbone interstrand NOEs in well-defined β-sheet structure, the strong, medium, and weak upper bounds were fixed to 2.5, 3.0, and 4.0 Å, respectively, in order to be consistent with the upper and lower limits used for hydrogen bonds. Upper limits corresponding to all the other long-range effects were fixed to 4.5 Å. Limits for distances involving methyl protons and nonstereospecifically assigned β-methylene protons were corrected as appropriate for center averaging (Wüthrich et al., 1983), and 0.5 Å was added to the upper distances involving methyl protons to account for the higher apparent intensity of methyl resonances (Wagner et al., 1987; Clore et al., 1987).

Furthermore, backbone NH···OC hydrogen bonds were identified according to the criteria of Wagner et al. (1987), which rely on the presence of NOEs between residues on opposite strands of an antiparallel β-sheet in connection with a slowly exchanging backbone amide proton. For each hydrogen bond, two distance restraints were used: 1.7–2.0 Å between the hydrogen and the oxygen acceptor atom and 2.7–3.0 Å between the nitrogen atom of the donor and the oxygen acceptor atom. Additional restraints were included in the distance geometry calculations to define the four disulfide bridges, i.e., ranges of 2.0–2.1 Å for $d$(S$^\gamma$,S$^\gamma$) and 3.0–3.1 Å for $d$(C$^\beta$,S$^\gamma$).

The φ angle restraints were derived from the $^3J_{NH-H\alpha}$ coupling constants. Angles corresponding to coupling constants larger than 8 Hz were constrained in intervals centered on −120° (from −120° ± 25° to −120° ± 55° according to the $^3J_{NH-H\alpha}$ values). Secondary structure determination was used to interpret eight additional coupling constants. In this case, an interval of ±35° was fixed around the presumed φ angle value. To obtain the $\chi_1$ angle restraints, the well-known Hilberts procedure was followed: the analysis of $^3J_{H\alpha-H\beta}$ coupling constants on the high-resolution DQF-COSY spectrum and of intraresidue NOEs on a 150-ms mixing time NOESY spectrum gave the stereospecific assignments of the β-protons. These assignments yielded the corresponding $\chi_1$ angles, restrained at an interval of ±45°. For H4, the $\chi_2$ angle was also deduced from NOE data. Correspondingly, an additional angle restraint of −90° ± 50° was used.

*Protocol for Structure Calculations.* As a first step, a number of three-dimensional structures were generated rapidly

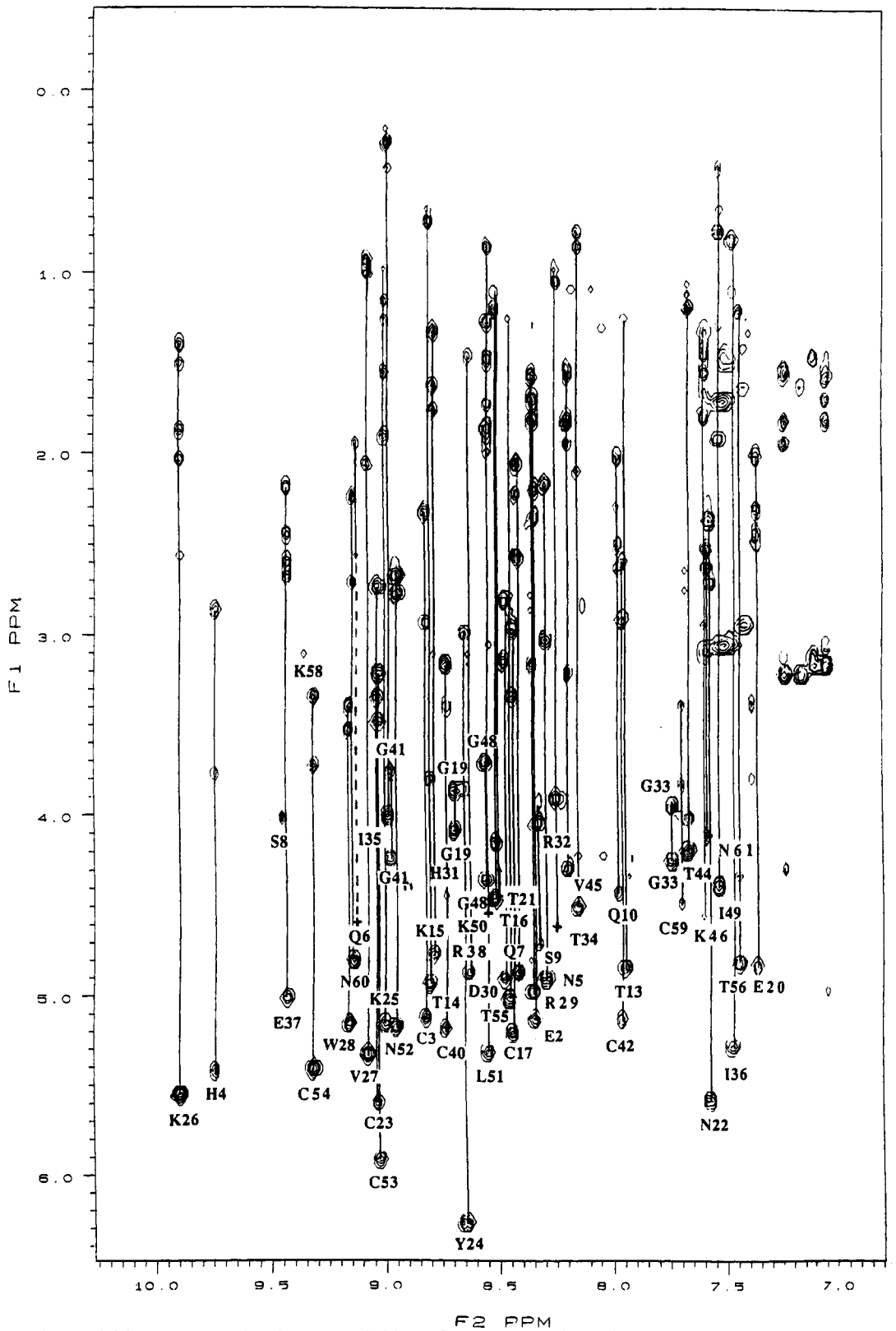


FIGURE 1: Part of the TOCSY spectrum of toxin $\alpha$, recorded in $H_2O$ at pH 3.5 and 45 °C. Only directly coupled cross-peaks are labeled.

on the basis of the amino acid sequence and the experimental restraints, using the DIANA program (Güntert et al., 1991). The analysis of the structures allowed the resolution of ambiguities in the assignment of NOE cross-peaks which arose form chemical shift degeneracy and thus the derivation of additional interproton restraints. This procedure was iterated several times by calculating at each stage a new set of structures with an improved list of restraints (Kraulis et al., 1990; Clore et al., 1990; Omichinski et al., 1990). The final set of structures and the final list of restraints were used for the structure refinement procedure, which consisted of simulated annealing calculations (Brünger et al., 1987) with the X-PLOR program (Brünger, 1988).

The target function was similar to that proposed by Nilges et al. (1988). It contained terms for bond lengths and bond angles, an improper-angle term restraining deviations from the planarity for the amide bonds and the aromatic rings, and square-well potentials to represent the NOE and torsion angle

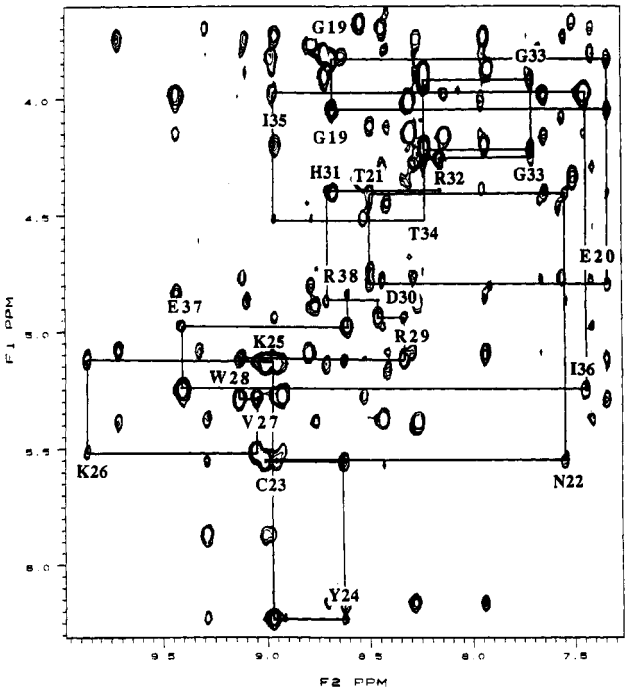


FIGURE 2: Part of the NOESY spectrum of toxin $\alpha$, recorded in $H_2O$ at pH 3.5 and 35 °C. The mixing time used is 300 ms. The assignments are shown, indicating the position of the COSY cross-peaks. The sequential $d_{\alpha N}$ connectivities are indicated for residues G19–R38.

restraints. It also contained a soft repulsive term instead of the van der Waals and electrostatic potentials. The simulated annealing protocol (Table I) was derived from the one described by Gippert et al. (1990) and is similar to the protocol already used in our laboratory (Bontems et al., 1992). It starts with an unrestrained minimization of the DIANA structure to improve its covalent geometry. The temperature is then linearly increased up to 1000 K during 2 ps, and in a consistent manner the values of the NOE and dihedral force constants are raised exponentially to 50 and 20 kcal/mol, respectively. A small value of the repulsive force constant is used in order to promote rearrangements in the structure. The structure is equilibrated for 4 ps. The repulsive force constant is in turn raised to 4 kcal/mol, and the structure is reequilibrated for 4 ps. The temperature is linearly decreased to 0 K during 4 ps, while the force field is gradually modified to be adapted with the temperature. Finally, 1 ps of restrained molecular dynamics is carried out with a standard energy function comprising an electrostatic term (Table I). This supplementary step is performed using a final temperature setting of 0 K. It allows us to get values for the energy terms comparable to those published previously. It also permits the final optimization of each structure.

Each DIANA structure took 1 h of computing time on an Alliant FX80; each X-PLOR structure needed 16 h to be calculated on the same computer. The resulting models were displayed and analyzed on an Evans and Sutherland PS390 using the SYBYL package.

## RESULTS AND DISCUSSION

### *Resonance Assignment*

The sequence-specific resonance assignment of toxin $\alpha$ was achieved according to a well-established procedure [see Wüthrich (1986) for a review].

*Spin System Identification.* The fingerprint region of the COSY spectra recorded in $H_2O$ at 308 and 318 K showed all but two of the NH–C$^\alpha$H cross-peaks expected. From the amide protons, relayed TOCSY connectivities (Figure 1) combined with COSY connectivities observed in both $H_2O$ and $D_2O$ allowed us to unambiguously identify most spin systems. Thus, five of the six lysines were recognized in the TOCSY experiment by two distinct series of connectivities correlating the side-chain protons to the backbone amide protons and the side-chain amide amino protons, respectively. For the remaining lysine, later identified as K58, TOCSY cross-peaks from the backbone NH proton to the $\beta$-, $\gamma$-, $\delta$-, and $\epsilon$-protons were not observed; therefore, this residue was recognized on the basis of the characteristic COSY and TOCSY patterns between the $\alpha$-, $\beta$-, $\delta$-, and $\gamma$-protons and of the NOESY correlations from the backbone NH proton to the side-chain protons.

The NOESY spectra were also helpful in assigning the side-chain amide protons of one glutamine and five asparagines on the basis of their N$^\epsilon$H$_2$–C$^\gamma$H$_2$ and C$^\delta$H$_2$–C$^\beta$H$_2$ cross-peaks, respectively, and the AMX spin-systems of aromatic residues on the basis of the NOE connectivities between the aromatic ring and the $\alpha$,$\beta$-protons.

From these assignments, we deduced that one of the two lacking NH–C$^\alpha$H cross-peaks corresponded to the AMX system of a nonaromatic residue, later recognized as D57, whose two C$^\alpha$H–C$^\beta$H$_2$ connectivities could be found on the COSY spectrum in $D_2O$. The last NH–C$^\alpha$H cross-peak missing corresponded to a leucine and was finally identified as the N-terminal residue of the polypeptide chain.

*Sequential Assignments.* Well-dispersed NOE connectivities were observed in the fingerprint region of NOESY spectra recorded with a mixing time of 300 ms at 308 and 318 K in $H_2O$; thus, the sequential assignments could be unambiguously determined on the basis of the $d_{\alpha N}$ connectivities (Figures 2 and 3). Tyrosine 24 was a convenient starting point: this residue is conserved in curaremimetic toxins and cardiotoxins from *Elapidae*, and its $\alpha$-proton has the same chemical shift (6.24 ppm) in all the published spectra. The ability to trace down connectivities in long sequences on the basis of the NH–C$^\alpha$H cross-peaks is illustrated in Figure 2 using residues G19–R38 as examples.

Moreover, each sequential dipeptide connectivity was confirmed at least by one additional $d_{\beta N}$ or $d_{NN}$ (Figure 3). Finally, the sequential assignments of the five proline residues were obtained on the basis of the strong NOE cross-peaks observed between the $\delta$-protons of each proline and the $\alpha$-proton of the preceding residue, and between the $\alpha$-proton of the proline and the backbone amide proton of the next residue. The whole sequence was thus assigned (see Table II).

### *Secondary Structure*

The prevalence of strong $d_{\alpha N}$ connectivities and large $^3J_{NH-H\alpha}$ coupling constants, along with the scarcity of $d_{NN}$ effects, indicates that the protein structure predominantly consists of extended segments of the polypeptide chain. A network of interstrand NH–C$^\alpha$H, NH–NH, and C$^\alpha$H–C$^\alpha$H NOEs and hydrogen bonds provide the evidence for arranging five individual strands into two antiparallel $\beta$-sheets. As shown in Figure 4, the $\beta$1- and $\beta$2-strands are involved in a double-stranded $\beta$-sheet, and the $\beta$3-, $\beta$4-, and $\beta$5-strands in a triple-stranded $\beta$-sheet, with the $\beta$3-strand surrounded by the $\beta$4- and $\beta$5-strands. These two $\beta$-sheets interact with each other by residues in the $\beta$1- and $\beta$4-strands; the long-range NOEs which connect residues 5–8 in $\beta$1 to residues 36–39 in $\beta$4 outline a small $\beta$-sheet motif.

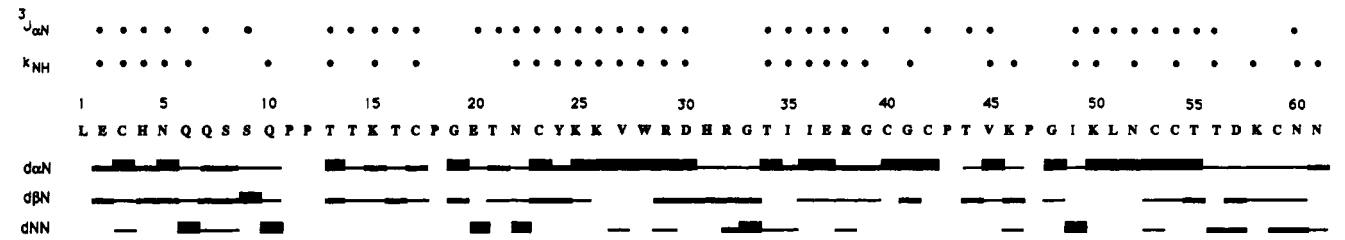


FIGURE 3: NMR data used for the sequence-specific assignment and the secondary structure identification. The data are compiled from the NOESY spectra recorded at 35 and 45 °C (pH 3.5, $T_m$ = 150 ms). $^3J_{\alpha N}$: (●) Vicinal coupling constants $^3J_{\alpha N} \geq 8$ Hz (glycine residues not included). $k_{NH}$: (●) Residues whose amide proton is not fully exchanged after 1 h in $D_2O$, at pH 3.5 and 25 °C.

A typical NOE pattern of a type I β-turn is found for residues 30–33, and typical NOE patterns of a type II β-turn are found for residues 17–20 and 46–49 (Figure 4). More strikingly, residues 7–10 show a NOE pattern consistent with a type II′ β-turn, i.e., a strong intraresidue NH($i$+1)–C$^\alpha$H($i$+1) effect, strong NH($i$+2)–NH($i$+3) and C$^\beta$H($i$+1)–NH($i$+2) effects, and no NH($i$+2)–NH($i$+3) effect.

### *Three-Dimensional Structure*

*Structural Statistics.* For the structure calculations, a final set of 409 distance constraints was used, including 46 intraresidue constraints (these were taken into account only when the information was not already contained in the angle restraints), 154 sequential and 157 long-range constraints, 40 distance restraints for 20 backbone hydrogen bonds, and 12 distance restraints for the four disulfide bridges. In addition, 49 $\phi$ angle, 23 $\chi_1$ angle, and one $\chi_2$ angle constraints were introduced. From the last 30 DIANA structures, eight were selected which presented no distance violation larger than 2 Å. These structures were further submitted to the refinement protocol, to yield the final structures.

The calculated structures are consistent with both the experimental data and the standard covalent geometry (Table III). In fact, no structure has a distance violation greater than 0.4 Å. The $\phi$ angles show no violation greater than 15°; only three residues (S9, I35, T56) have deviations of 5–15° from the $\phi$ angle restraints in more than one structure. The $\chi_1$ angle restraints are always satisfied. Furthermore, the covalent geometry is correct, as can be judged by the low ⟨rmsd⟩ values for the bond lengths (0.014 Å) and for the angles (3.22°). The van der Waals energy is large and negative (average value: −234 kcal/mol), which indicates that there are no bad nonbonded contacts.

The analysis of the Ramachandran plot (Figure 5) shows that the $\phi,\psi$ angle values of the calculated structures are in the allowed regions. Most residues are present in the β-strand region of the plot. A few residues have $(\phi,\psi)$ values in the α-helix region. These are either residues located at the edges of the β-sheets (T21, T55) or at the C-terminal part of the molecule (C59) or residues which belong to a type I turn (H31, R32). In the $\phi > 0$ part of the plot, S8 falls in the region generally allowed for residues at position $i$+1 of type II′ β-turns. K58 shows $\phi,\psi$ angle values consistent with an $i$+2 position in type II β-turns; the β-turn involving K58 will be described later. Four out of the five glycines are finally found at the limits of the glycine-allowed region. G39 is the only glycine to be represented in a region of the plot allowed for most of the amino acids.

*Description of the Backbone Structure.* All the calculated structures of toxin α possess a very similar backbone folding. The average rms deviation value for the coordinates of the backbone atoms is 0.8 Å in the eight structures (0.51 Å between the eight structures and the average structure). Superpositions of the backbone structures are shown in Figure 6a,b. The folding of the polypeptide chain mainly results in a long central loop surrounded by two shorter loops. Loop 1 includes the β1- and β2-strands. Loop 2 includes the β3- and β4-strands. Loop 3 includes the β5-strand and has the interesting feature of being oriented almost perpendicularly to loops 1 and 2. An additional six-residue loop is formed by the C-terminal part of the polypeptide chain. The four loops arise from a region cross-linked by the four disulfide bridges. Finally, the side view of toxin α (Figure 6b) clearly indicates that the molecule is slightly concave. The short C-terminal loop is found on its convex side, in a plane parallel to the plane defined by loops 1 and 2.

*β-Sheets.* Loops 2 and 3 contain the antiparallel triple-stranded β-sheet (β3-, β4- and β5-strands). Analysis of the $(\phi,\psi)$ distribution (Figure 5) shows that the β-sheet involves the residues C23–R29, T34–C40, and I49–C54. The three β-strands form a plane which is slightly twisted at the tip of loop 2 (see Figure 6b). Loop 1 contains the double-stranded β-sheet (β1- and β2-strands). The sheet shows a regular structure between residues E2–H4 and T14–T16. A pseudo-β-bulge is found between the β-sheet and the turn at positions 7–10. It involves residues Q6, P11, and P12, which have β conformations. A distortion of the β1-strand is found at the position of N5, as detected by the short distance measured between the two amide protons of N5 and Q6 (<3.0 Å) and by the $\psi$ angle value of N5 (60° ± 10°). Because of this structural irregularity, the small β-sheet formed by residues in the β1-strand (loop 1) and residues in the β4-strand (loop 2) has classical $\phi,\psi$ angle values only for Q7 and E37.

*β-Turns.* Five β-turns are found in toxin α. The 30–33 turn is close to a type I β-turn, but its $\psi(i+2)$ angle is between −20° and −60°. Thus, the $i \rightarrow i+3$ hydrogen bond corresponding to this β-turn is not observed in most structures. The (17–20) and the (46–49) turns are type II β-turns (Figure 5), which both have the $i \rightarrow i+3$ hydrogen bond. The 7–10 turn is close to a type II′ β-turn and also has the $i \rightarrow i+3$ hydrogen bond. Finally, the fifth β-turn is found between residues 56 and 59, in the small C-terminal loop. This β-turn can be characterized as a type II turn on the basis of its $\phi(i+1)$, $\phi(i+2)$, and $\psi(i+1)$ angle values, but its $\psi(i+2)$ angle is between 30° and 60°; thus, the $i \rightarrow i+3$ hydrogen bond is not observed in most structures.

*Deviations from the Average Structure.* Figure 7 presents the backbone and side-chain ⟨rmsd⟩ values as a function of the residue number. It displays five regions which show remarkably low ⟨rmsd⟩ values for the backbone atoms (<0.4 Å). These regions correspond to the β-strands of the triple- and the double-stranded β-sheets. The conformations of the disulfides also appear to be well-defined. For three disulfides, the $\chi_1$ angle values were determined from the NMR data and introduced as restraints in the calculations. Thus, the bridge

Table II: Proton Chemical Shifts of Toxin α at 45 °C and pH 3.5[a]

| residue | chemical shift (ppm) of | | | | |
|---|---|---|---|---|---|
| | NH | Hα | Hβ | Hγ | others |
| Leu1 | | 4.15 | 1.58 | 1.46 | $C^{\delta}H_3$ 0.71, 0.62 |
| Glu2 | 8.31 | 5.09 | 1.80, 1.70 | 2.34, 2.17 | |
| Cys3 | 8.81 | 5.09 | 2.9, 2.3 | | |
| His4 | 9.72 | 5.37 | 3.75, 2.85 | | $C^{2}H$ 8.89; $C^{4}H$ 6.77 |
| Asn5 | 8.28 | 4.87 | 3.00, 2.15 | | $N^{\delta 2}H_2$ 7.54, 7.01 |
| Gln6 | 9.32 | 4.57 | 2.56, 1.92 | 2.02 | $N^{\epsilon 2}H_2$ 6.58, 7.70 |
| Gln7 | 8.39 | 4.83 | 2.20, 2.04 | 2.55 | |
| Ser8 | 9.44 | 3.98 | 4.15, 4.05 | | |
| Ser9 | 8.32 | 4.68 | 4.01 | | |
| Gln10 | 7.95 | 4.39 | 2.26, 2.00 | 2.60, 2.49 | |
| Pro11 | | 4.58 | 2.35, 1.78 | 2.15 | $C^{\delta}H_2$ 3.83, 3.63 |
| Pro12 | | 3.89 | 1.85 | 2.05 | $C^{\delta}H_2$ 3.81, 3.58 |
| Thr13 | 7.92 | 4.80 | 4.50 | 1.23 | |
| Thr14 | 8.80 | 4.89 | 3.77 | 0.70 | |
| Lys15 | 8.75 | 4.72 | 1.75, 1.6 | 1.3 | $C^{\delta}H_2$ 1.68; $C^{\epsilon}H_2$ 3.07; $N^{\zeta}H_2$ 7.50 |
| Thr16 | 8.49 | 4.44 | 4.11 | 1.19 | |
| Cys17 | 8.43 | 5.16 | 3.30, 2.92 | | |
| Pro18 | | 4.40 | 2.26, 1.98 | 2.11 | $C^{\delta}H_2$ 3.77, 3.63 |
| Gly19 | 8.67 | 4.05, 3.85 | | | |
| Glu20 | 7.34 | 4.79 | 2.29, 1.99 | 2.45 | |
| Thr21 | 8.50 | 4.40 | 4.38 | 1.15 | |
| Asn22 | 7.57 | 5.55 | 2.68, 2.35 | | $N^{\delta 2}H_2$ 6.94, 6.23 |
| Cys23 | 9.02 | 5.55 | 3.34, 2.70 | | |
| Tyr24 | 8.64 | 6.24 | 3.83, 2.95 | | $C^{\delta}H$ 6.72; $C^{\epsilon}H$ 6.54 |
| Lys25 | 8.97 | 5.10 | 1.89, 1.54 | 1.25 | $C^{\delta}H_2$ 1.13; $C^{\epsilon}H_2$ 2.80; $N^{\zeta}H_2$ 7.87 |
| Lys26 | 9.86 | 5.50 | 2.01, 1.85 | 1.49 | $C^{\delta}H_2$ 1.38; $C^{\epsilon}H_2$ 2.53 |
| Val27 | 9.04 | 5.29 | 2.04 | 0.99, 0.92 | |
| Trp28 | 9.15 | 5.11 | 3.50, 3.35 | | $C^{\delta 1}H$ 7.04; $C^{\epsilon 3}H$ 7.36; $C^{\zeta 3}H$ 6.84; $C^{\eta 2}H$ 7.20; $C^{\zeta 2}H$ 7.46 |
| Arg29 | 8.33 | 4.94 | 1.80, 1.68 | 1.55 | $C^{\delta}H_2$ 3.13; $N^{\eta 2}H_2$ 7.03 |
| Asp30 | 8.47 | 4.87 | 3.12, 2.78 | | |
| His31 | 8.72 | 4.40 | 3.35 | | $C^{2}H$ 8.67; $C^{4}H$ 7.42 |
| Arg32 | 8.16 | 4.25 | 1.93, 1.80 | 1.52 | $C^{\delta}H_2$ 3.19; $N^{\eta 2}H_2$ 7.20 |
| Gly33 | 7.72 | 4.22, 3.92 | | | |
| Thr34 | 8.23 | 4.51 | 3.87 | 1.06 | |
| He35 | 8.95 | 3.96 | 0.28 | 0.90, 0.71, 0.32 ($CH_3$) | $C^{\delta}H_3$ 0.40 |
| Ile36 | 7.45 | 5.24 | 1.48 | 1.46, 1.09, 0.80 ($CH_3$) | $C^{\delta}H_3$ 0.80 |
| Glu37 | 9.41 | 4.96 | 2.41, 2.18 | 2.65, 2.57 | |
| Arg38 | 8.59 | 4.84 | 1.25 | 1.60, 1.44 | $C^{\delta}H_2$ 3.14, 3.08; $N^{\eta 2}H_2$ 7.08 |
| Gly39 | 6.16 | 3.90, 3.80 | | | |
| Cys40 | 8.72 | 5.14 | 3.12 | | |
| Gly41 | 8.96 | 4.20, 3.74 | | | |
| Cys42 | 7.96 | 5.10 | 2.90, 2.58 | | |
| Pro43 | | 4.40 | 1.92, 1.68 | 0.95, 0.81 | $C^{\delta}H_2$ 2.92, 2.85 |
| Thr44 | 7.64 | 4.15 | 3.98 | 1.17 | |
| Val45 | 8.13 | 4.46 | 2.09 | 0.84, 0.76 | |
| Lys46 | 7.57 | 4.51 | 1.79, 1.54 | 1.42 | $C^{\delta}H_2$ 1.42; $C^{\epsilon}H_2$ 2.91; $N^{\zeta}H_2$ 7.39 |
| Pro47 | | 4.33 | 2.31, 1.85 | 1.99, 2.10 | $C^{\delta}H_2$ 3.80, 3.56 |
| Gly48 | 8.54 | 4.31, 3.67 | | | |
| Ile49 | 7.51 | 4.35 | 1.90 | 1.27, 0.90, 0.75 ($CH_3$) | $C^{\delta}H_3$ 0.41 |
| Lys50 | 8.52 | 4.50 | 1.98, 1.90 | 1.70 | $C^{\delta}H_2$ 1.46; $C^{\epsilon}H_2$ 3.02; $N^{\zeta}H_2$ 7.50 |
| Leu51 | 8.51 | 5.26 | 1.84, 1.26 | 1.46 | $C^{\delta}H_3$ 0.84 |
| Asn52 | 8.94 | 5.14 | 2.75, 2.65 | | $N^{\delta 2}H_2$ 7.65 |
| Cys53 | 9.02 | 5.86 | 3.45, 3.20 | | |
| Cys54 | 9.30 | 5.37 | 3.70, 3.34 | | |
| Thr55 | 8.43 | 4.97 | 4.79 | 1.22 | |
| Thr56 | 7.42 | 4.77 | 4.30 | 1.20 | |
| Asp57 | 8.45 | 4.63 | 2.70, 2.50 | | |
| Lys58 | 9.33 | 3.07 | 1.85, 1.75 | 1.00 | $C^{\delta}H_2$ 0.50; $C^{\epsilon}H_2$ 2.80 |
| Cys59 | 7.69 | 4.44 | 3.80, 3.35 | | |
| Asn60 | 9.12 | 4.76 | 2.70, 2.20 | | $N^{\delta 2}H_2$ 7.95, 8.29 |
| Asn61 | 7.58 | 4.09 | 2.60, 2.50 | | $N^{\delta 2}H_2$ 7.39, 6.58 |

[a] Shifts were measured ±0.02 ppm relative to sodium 3-trimethylsilyl-[2,2,3,3-$^2H_4$]propionate.

(42, 53) has an unique right-handed conformation (Richardson, 1981), and the bridges (3, 23) and (54, 59) have two sets of conformations corresponding to $\chi_3 = \pm 90°$. Moreover, although the $\chi_1$ angle of C40 could not be constrainted, the bridge (17, 40) has the same right-handed conformation in six structures, with $\chi_1$ (C40) = −70°.

In contrast, two regions show large average ⟨rmsd⟩ values in both the backbone and the side chains. The less defined region corresponds to the tip of loop 2. Closer inspection of loop 2 shows that the backbone conformation of the β-turn (30–33) is well-defined, but the orientation of the β-turn with respect to the rest of loop 2 is significantly less well-defined. This may be caused by the flexibility of G33. The second region of the toxin that shows a high average ⟨rmsd⟩ in both the backbone and the side chains comprises residues 44–48, which correspond to the external part of loop 3. The side chains located in these two poorly resolved regions of toxin α are fully exposed to the solvent.

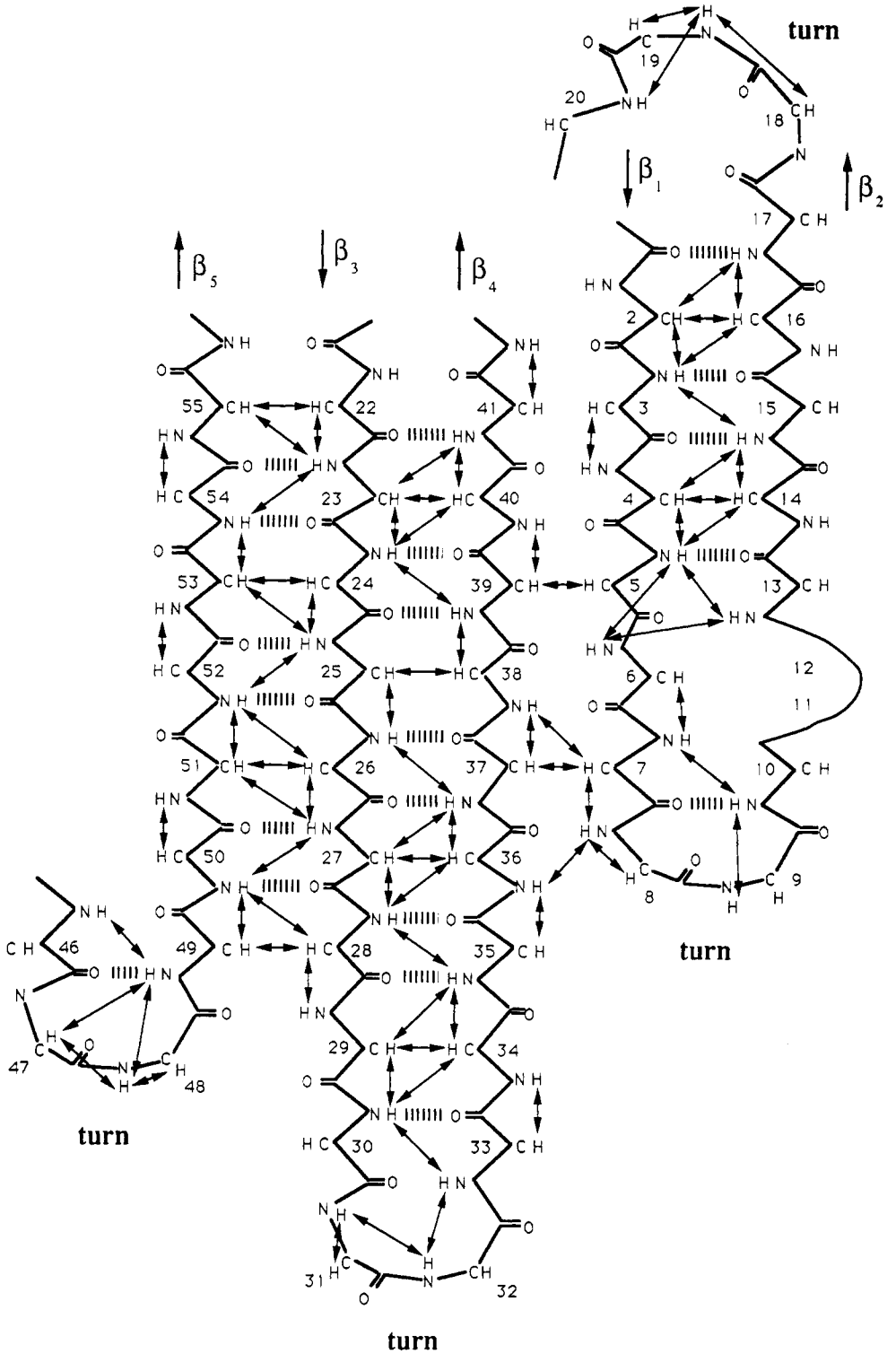


FIGURE 4: Antiparallel β-sheets and turns in toxin α. The NOEs used to establish the position of the strands are indicated by double-headed arrows. The dashed lines correspond to the hydrogen bonds identified on the basis of the amide proton exchange rates and of the interstrand NOEs.

*Description of Side Chains.*

*Role of Buried Residues.* A series of individual side chains corresponding to the eight half-cystines, H4, Y24, K26, R38, and N60 shows a low surface accessibility in toxin α. These side chains are well-defined (⟨rmsd⟩ <1 Å, see Figure 7), due to the large number of constraints available involving both the backbone and side-chain protons. They are found in the upper part of the molecule (see Figure 6c) and appear to play important structural roles.

The four disulfides are clustered together and form a highly constrained structure (Figure 6c). Three of them clearly contribute to the stability of the three large loops: the bridges (3, 23) and (17, 40) link loop 1 to loop 2, and the bridge (42, 53) links loop 3 to loop 2. The bridge (54, 59) stabilizes the smaller loop formed by the C-terminal part of the polypeptide chain.

The side chains of H4 and N60 seem to contribute to the positioning of the C-terminal loop with respect to the rest of the molecule. In fact, the side chain of H4, which belong to

Table III: Structural Statistics[a]

| |
|---|
| ⟨*E*(total)⟩ = −1940 ± 53 kcal/mol |
| ⟨*E*(elec)⟩ = −2164 ± 41 kcal/mol |
| deviations from experimental restraints[b] |
| ⟨*E*(NOE)⟩ = 4.11 ± 2.60 kcal/mol |
| ⟨*E*(Cdihe)⟩ = 2.73 ± 1.33 kcal/mol |
| deviations from idealized geometry |
| ⟨rmsd(bond)⟩ = 0.014 ± 0.001 Å |
| ⟨rmsd(angle)⟩ = 3.224° ± 0.052° |
| ⟨rmsd(improper)⟩ = 0.488° ± 0.037° |
| ⟨rmsd(dihe)⟩ = 22.563 ± 0.075° |
| ⟨*E*(L-J)⟩[c] = −234 ± 6 kcal/mol |

[a] All the values are averaged on the eight X-PLOR structures, and, for each value, the maximal range is specified. [b] The values of the square-well NOE and dihedral angle potentials are calculated with force constants of 25 kcal/mol·Å$^2$ and 20 kcal/mol·rad$^2$, respectively. [c] *E*(L-J) is the Lennard-Jones van der Waals energy calculated with the CHARMM (Brooks et al., 1983) empirical function.

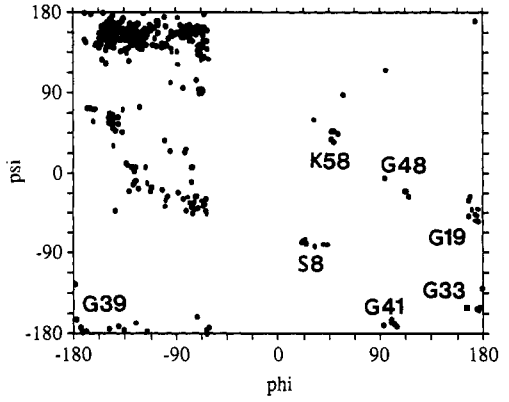


FIGURE 5: Ramachandran $\phi,\psi$ plot for the residues of the eight X-PLOR structures.

loop 1, shows a well-defined orientation (⟨rmsd⟩ ≈ 0.5 Å; numerous NOEs between the imidazole ring and the side chains of T14, K58, and N61) and forms several van der Waals contacts within loop 1 (T14) and with the C-terminal part (K58, N61) of toxin α. Similar interactions have been observed for the analogous F4 in α-cobratoxin (Betzel et al., 1991). Moreover, the side chain of N60, which is located in the C-terminal tail, is directed toward the interior of the molecule (Figure 6c), being even better defined than the main chain (⟨rmsd⟩ ≈ 0.4 Å; several NOEs with the H4, Y24, and G39 amide protons and with the side chain of R38). This side chain shares numerous van der Waals contacts with the side chains of residues from loop 1 (C3) and from loop 2 (K25, R38). A detailed inspection of the structures shows that, in some of them, the γ-amide group of N60 is also involved in hydrogen bonds with the backbone atoms of the upper parts of loop 1 or loop 2. Similar interactions have been described for the analogous N61 in erabutoxin b (Low & Corfield, 1986), and similar hydrogen bonds have been observed for the analogous N63 in α-cobratoxin (Betzel et al., 1991).

Tyrosine 24, which is located on the concave face of loop 2 (Figure 6c), has a well-defined orientation in our structures (⟨rmsd⟩ ≈ 0.3 Å; numerous NOEs with the C42, P43, and K26 side-chain protons and with the G39, C40, and K26 backbone protons); it is surrounded by the polypeptide chain (37–43) which connects loop 2 to loop 3 and shows several van der Waals interactions with the side chains of P43, E37, and K26 (Figure 8b). The three latter side chains form a cluster with the tyrosyl ring. Such a cluster has already been observed around the analogous Y25 in erabutoxin b (Low & Corfield, 1986), and a similar hydrophobic environment has been described for the analogous Y21 in α-cobratoxin (Le Goas et al., 1992). Moreover, our NMR data show that the tyrosyl ring has a hindered rotation in toxin α: at 65 °C, the aromatic proton resonances form an AA'BB'type spectrum (Wüthrich, 1976) and broaden extensively when the temperature is lowered to 15 °C (data not shown). In view of its conservation in all toxins studied so far, the cluster of Y24 probably contributes to the stability of the upper part of loop 2 and of the strand (37–43) connecting loop 2 to loop 3 (Figure 8b). It may also be essential for the folding of this region of the molecule.

Thus, the numerous interactions involving the buried residues of toxin α suggest that H4, Y24, and N60 play, together with the eight half-cystines, a central role in the tertiary structure organization of the molecule.

*Role of Hydrophobic Residues.* Interestingly, the hydrophobic side chains of toxin α are not found among the most buried side chains of the molecule, even though they show reduced surface accessibilities. Except V45, their positions are again well-defined (see Figure 7) due to the numerous NOEs observed.

L1 is spatially isolated from the other hydrophobic residues of the molecule. It is located in the double-stranded β-sheet and is surrounded from one side by the polypeptide chain at 17–23 and from the other side by the polypeptide chain at 55-57 (Figure 8a). Thus, on one hand, its side chain makes van der Waals contacts with the main chain of residues T21 and N22. This should contribute to the structural stability of the polypeptide chain connecting loop 1 to loop 2. On the other hand, van der Waals contacts between the side chains of L1 and D57, in addition to electrostatic interactions between the side chains of E2 and K58, might contribute to the structural stability of the C-terminal chain.

The remaining hydrophobic residues, i.e., V27, W28, I35, I36, V45, I49, and L51, are all found in the central part of the triple-stranded β-sheet, and their side chains are distributed on both sides of the molecule (see Figure 6c). On the concave side, W28 appears as the central residue around which is organized the compaction of the side chains of K26, D30, I35, E37, and I49. Its large and hydrophobic side chain is particularly well-defined (⟨rmsd⟩ ≈ 0.4 Å; numerous NOEs with side chains of residues K26, D30, I35, E37, and I49) and is clustered between I35 in loop 2 and I49 in loop 3 (see Figure 6c). Analogous clusters have been described around W29 in erabutoxin b (Low & Corfield, 1986) and around W25 in α-cobratoxin (Le Goas et al., 1992). The hydrophobic interactions involved in these clusters may be essential for the stability of the concave face of the triple-stranded β-sheet. They may also be involved in the folding of the triple-stranded β-sheet; however, it has recently been demonstrated that, in erabutoxin b, W29 can be replaced by F or H without preventing the correct folding of the toxin main chain (Pillet et al., personal communications). Two other hydrophobic residues, i.e., V45 and L51, are located in loop 3 of toxin α. Their side chains are directed toward the center of the loop, thus forming a local hydrophobic environment. V45 is the only hydrophobic residue to show a badly defined side chain (⟨rmsd⟩ ≈ 1.6 Å), probably because of its position at the external part of the loop, in a region exposed to the solvent. Finally, on the convex face of the molecule, the well-defined side chains of V27 and I36 share numerous van der Waals interactions. The compaction of hydrophobic side chains on either side of the molecule are expected to contribute to the stability of the central parts of loops 2 and 3.

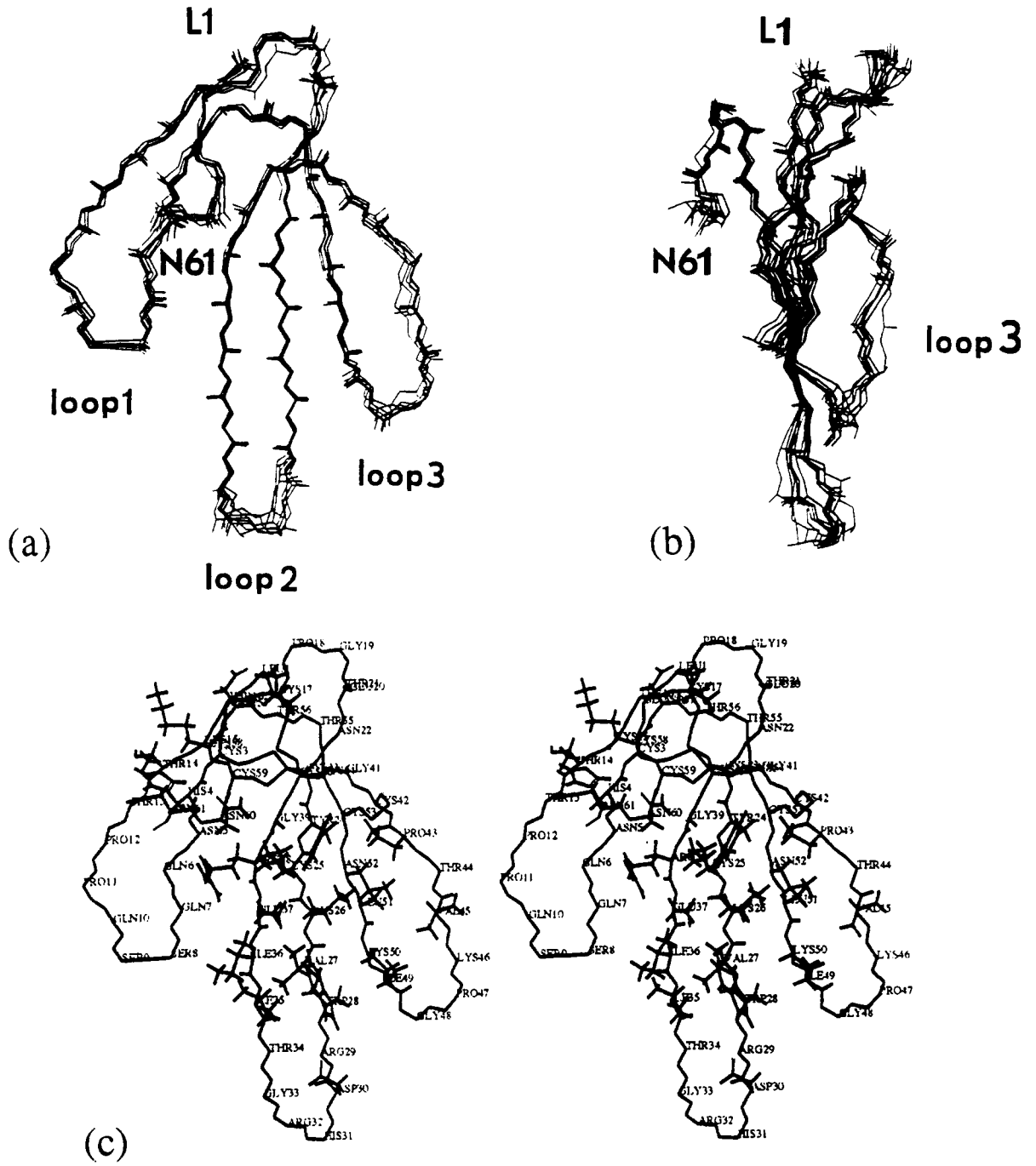


FIGURE 6: (a) Superposition of the backbone atoms of the eight solution structures of toxin α: view toward the five-strand β-sheet and side view, perpendicular to the previous one. (b) Stereoview of the backbone of toxin α, with the four disulfides and the following side chains: L1, H4, T14, Y24, K25, K26, V27, W28, D30, I35, I36, E37, R38, P43, V45, I49, L51, D57, K58, N60, and N61.

### *Comparison with the Crystal Structure of Erabutoxin b*[2]

Erabutoxin b from *L. semifasciata* (62 residues, four disulfides) is another member of the family of the curaremimetic toxins from snake venom. Its primary sequence differs from that of toxin α by 16 amino acid substitutions and by the deletion in toxin α of one residue located between C17 and P18. The crystal structure of erabutoxin b has been elucidated in different laboratories (Low et al., 1976; Tsernoglou & Petsko, 1976) and has been refined to 1.4-Å resolution (Bourne et al., 1985; Smith et al., 1988).

[2] The residues of toxin α and erabutoxin b are numbered according to their respective sequential positions. Due to the mutation/deletion process, there is a shift in the numbering by one residue between the two toxins starting after C17.

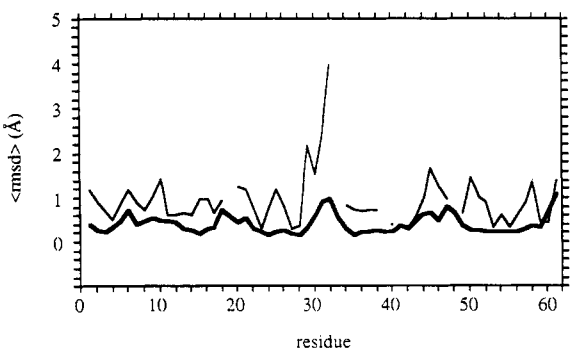


FIGURE 7: Average atomic ⟨rmsd⟩ of the eight X-PLOR structures about the mean structure calculated for the backbone (thick line) and the side-chain (thin line) atoms as a function of residue number.

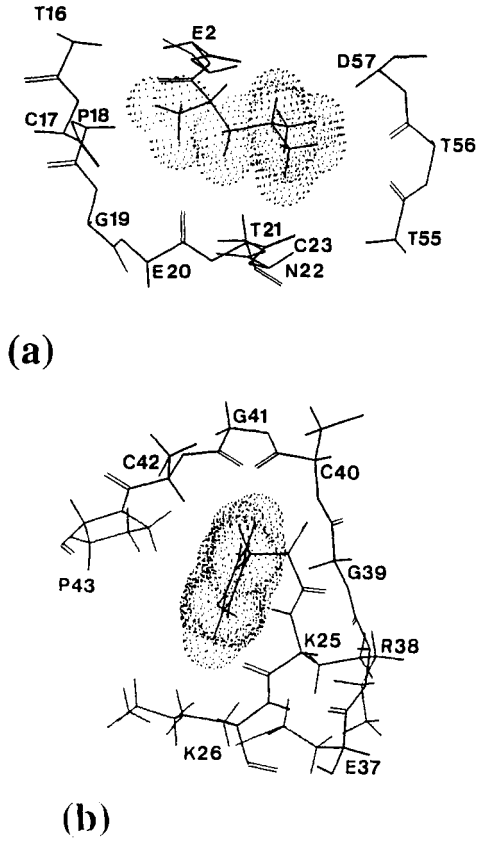


FIGURE 8: Leucine 1 (a) and tyrosine 24 (b) with their surrounding amino acids in an NMR-derived structure of toxin $\alpha$.

*Global Backbone Superposition.* The backbone superposition of the solution structure of toxin $\alpha$ and the crystal structure of erabutoxin b (Smith et al., 1988) clearly illustrates that the three-dimensional structures of these two analogous proteins are very similar (Figure 9). The ⟨rmsd⟩ calculated between the eight backbone structures (1, 61) of toxin $\alpha$ and the corresponding peptide segments {(1, 17) + (19, 62)} in erabutoxin b is equal to 1.71 Å. The structural similarity between the two toxins is quantitatively illustrated by the comparison of the $\phi,\psi$ angle values of residues at the corresponding sequential positions in toxin $\alpha$ and in erabutoxin b (Figure 10). Only a few $\phi$ and $\psi$ angles differ between the two toxins. C17, at the position preceding the deletion in toxin $\alpha$, is one of the most affected residues. In fact, in toxin $\alpha$, C17 is in position $i$ of the type II $\beta$-turn (C17, P18, G19, E20), whereas in erabutoxin b C17 precedes the type II $\beta$-turn (S18, P19, G20, E21). Thus, the deletion of S18 in toxin $\alpha$ is partly compensated by the substitution of S18 with C17 at position $i$ of the $\beta$-turn, and the global fold of the toxin is conserved. During the crystallization experiments, erabutoxin b was at pH 9.5, which is far from the pH of this study. However, according to previous NMR data recorded on analogous toxins (Hider et al., 1982; Bystrov et al., 1983; Kondakov et al., 1984), and to fluorescence experiments made on toxin $\alpha$ (Ménez et al., 1980), the pH is not expected to influence the overall structure of toxin $\alpha$.

A few minor structural differences between the crystal and solution structures are observed in loop 1 and in the C-terminal part of the chain. They might be a consequence of the deletion of S18 in toxin $\alpha$, which shortens the $\beta$2-strand. Thus, in erabutoxin b, loop 1 is about 1 Å closer to both loop 2 and to the C-terminal part than it is in toxin $\alpha$ (Figure 9). Also, two hydrogen bonds have been found in erabutoxin b between loops 1 and 2 (Bourne et al., 1985). The first one involves the amide proton of S8 in loop 1 and the carbonyl oxygen of I37 in loop 2, and the second one links the carbonyl oxygen atom of Q6 to the side-chain NH of R39. No experimental evidence has been obtained for the existence of such a main-chain hydrogen bond involving the amide of S8 in toxin $\alpha$. In fact, this amide proton is fully exchanged in less than 30 min at 25 °C and pH 3.5. In contrast, the main-chain/side-chain hydrogen bond linking the carbonyl oxygen atom of Q6 to the side-chain NH of R38 is found in two of the eight structures of toxin $\alpha$; it is consistent with the distance measured between loops 1 and 2. Finally, since the C-terminal chain is in contact with loop 1 through numerous electrostatic interactions, a small difference in the positioning of the C-terminal chain in the two toxins is observed in relation to the difference in the position of loop 1.

*Structural Mobility.* The variations of the ⟨rmsd⟩ values in toxin $\alpha$ and the backbone $B$ factors in erabutoxin b are remarkably correlated (Figure 11). The regions associated with the largest $B$ factors in the crystal structure correspond to poorly resolved regions in the solution structure. In fact, the crystallographic $B$ factors provide a measure of the mean-square displacements of the atoms in the crystal, while the ⟨rmsd⟩ values provide a measure of the precision of the atomic positions in the calculated solution structures. The precision in the NMR structures is related to the number of short (<5 Å) experimental interproton distances. However, in the solvent-exposed turns and loops, the number of observed interproton distances is limited. This reflects a reduction of nonbonded contacts, and thus of the packing interactions, which may be related to an increased atomic mobility (Clore & Gronenborn, 1991). Interestingly, notable differences are found for the two parameters in the R29–T34 region corresponding to the tip of loop 2: the backbone seems to be fixed in the crystal, while it shows a high ⟨rmsd⟩ (up to 1.8 Å) in the solution structures; the side chains of R29, H31, and R32 all have $B$ factors smaller than 22 Å$^2$ in the crystal, whereas they are poorly resolved in the solution structures. These different properties may be related to the two following observations. First, the tip of loop 2 is a solvent-exposed region in toxin $\alpha$. Thus, only a limited number of short interproton contacts is observed between residues R29–T34 and residues in other parts of the molecule; this may be associated with a large mobility of the corresponding polypeptide chain. Second, the analysis of the crystal packing diagram of erabutoxin b (Low et al., 1976) shows that the edge of loop 2 is involved in close intermolecular contacts. Thus, the R29–T34 region may show a restricted mobility in the erabutoxin crystal because of the packing interactions.

*Side-Chain Superposition.* Analogously to the conservation of the three-dimensional structure of the backbone of these toxins, a close structural organization is observed for the respective side chains. In particular, the disulfide bridges are located similarly. The preferred conformation of the disulfides (3, 23) and (42, 53) in toxin $\alpha$ is the conformation found in erabutoxin b, and the conformation of the disulfide (54, 59) of erabutoxin b is found in three solution structures. In contrast, the bridge (17, 40) of toxin $\alpha$ shows $\chi_3$ values systematically opposite to that found in erabutoxin b.

The 16 mutated amino acids are equally distributed in the three-dimensional structure of toxin $\alpha$: L/R1, E/I2, H/F4, Q/H6, and P/Q12 are located in loop 1, T/S21, N/S22, K/H25, V/Q27, R/S29, and H/F31 are located in loop 2, N/S52 is located in loop 3, and T/E55, T/S56, D/E57, and K/V58 are located in the smaller C-terminal loop. Interestingly, the spatial orientations of these side chains in toxin

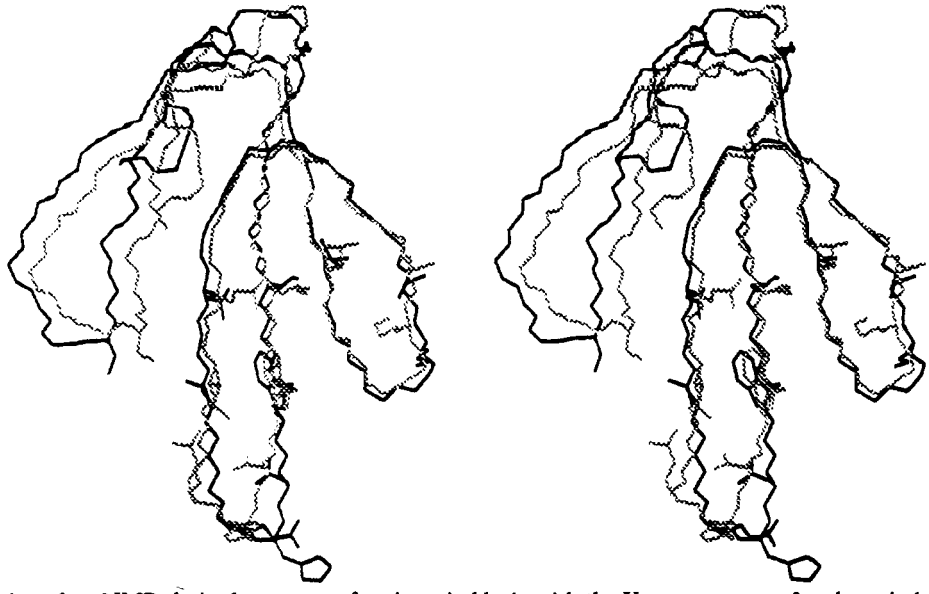

FIGURE 9: Superposition of an NMR-derived structure of toxin α, in black, with the X-ray structure of erabutoxin b, in gray. Stereoview of the backbones, with the side chains assigned to the toxic site of curaremimetic toxins, i.e., S8, K26, W28, D30, H/F31, R32, G33, I35, E37, V45, K46, G48, and L51. Atomic coordinates of erabutoxin b are from the Protein Data Bank, Brookhaven National Laboratory (reference: 3EBX, R3EBXSF).

α fit generally well with the positions of the corresponding side chains in erabutoxin; only four of these side chains show different $\chi_1$ angles in the two toxins, i.e., the side chains of P12, K25, N52, and T55 (Figure 10). Furthermore, the mutations do not seem to perturb the conformations of the neighboring amino acids. In particular, most conserved residues have the same $\chi_1$ angle in the two toxins. Only three conserved residues (Q7, K15, E20) show systematically different $\chi_1$ angles (Figure 10).

*The Toxic Site.* None of the mutated residues is found on the concave side of toxin α. This supports the previous assumption that the toxic site of a curaremimetic toxin is located on its concave side. Indeed, on the basis of various considerations, which include the sequence comparisons of homologous toxins (Low et al., 1976; Karlsson et al., 1979; Endo & Tamiya, 1987) and chemical modifications (Ménez et al., 1982; Faure et al., 1983; Ménez et al., 1986), the toxic site of a curaremimetic toxin has been located essentially in loops 2 and 3, with the side chains of critical residues pointing toward the concave side of the molecule (Figure 9). Interestingly, only three side chains belonging to this site, i.e., W28, I35 and E37, show a good spatial definition (a low ⟨rmsd⟩ and a unique $\chi_1$ rotamer) in the solution structure of toxin α. The positions of these three side chains in toxin α fit very well with the positions of the corresponding side chains in erabutoxin b (Figure 9). The eight remaining side chains which belong to the presumed toxic site are poorly resolved in the solution structure of toxin α: D30, H/F31, R32, V45, K46, and L51 are characterized by a side-chain ⟨rmsd⟩ higher than 1, and S8, K26, D30, H/F31, R32, and V45 have a large distribution of $\chi_1$ rotamers. For these side chains, the crystal conformation constitutes one of the conformations which exist in the solution structures.

In conclusion, the study reported in the present paper clearly establishes that toxin α is folded like erabutoxin b, in agreement with previous proposals (Ménez et al., 1976; Dufton & Hider, 1977; Ménez, 1991). However, it also shows that the two toxins have some differences, in particular around the region where an amino acid deletion occurs. Examination of the spatial organization of the two molecules confirms that the side chains conserved in the two toxins are predominantly

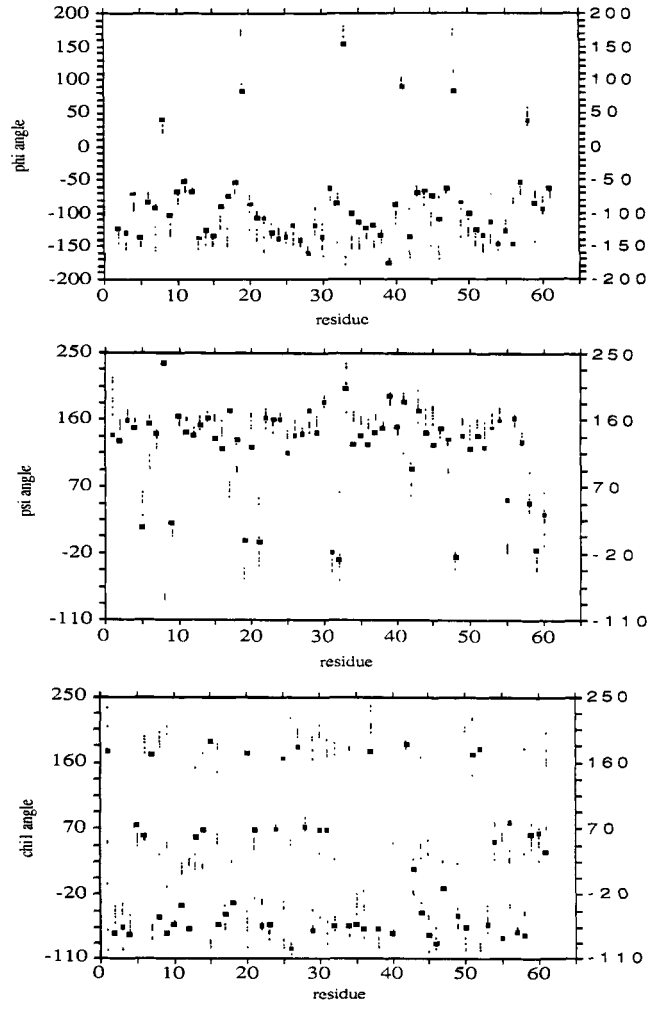


FIGURE 10: $\phi,\psi$ and $\chi_1$ angle values measured for each residue of the eight X-PLOR structures of toxin α. The superimposed large points correspond to the $\phi,\psi$ and $\chi_1$ angle values measured on the X-ray structure of erabutoxin b. The sequences of toxin α and erabutoxin b have been matched by deleting S18 from the erabutoxin sequence. Atomic coordinates of erabutoxin b are from the Protein Data Bank, Brookhaven National Laboratory (reference: 3EBX, R3EBXSF).

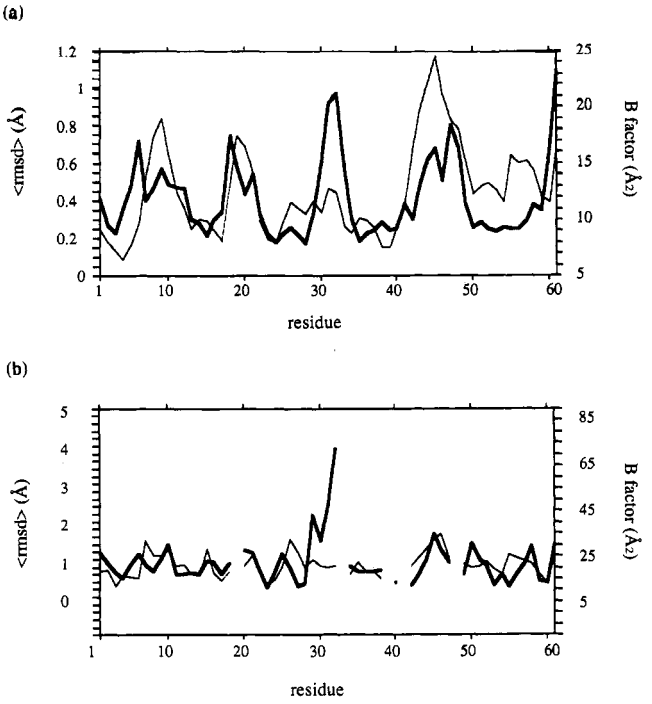


FIGURE 11: Comparison of the average atomic ⟨rmsd⟩ of the eight X-PLOR structures about the mean structure (thick line) calculated for the backbone (a) and the side-chain (b) atoms, with the *B* factors of the corresponding atoms in erabutoxin b (thin line). The sequences of toxin α and erabutoxin b have been matched by deleting S18 from the erabutoxin sequence. *B* factors of erabutoxin b are from the Protein Data Bank, Brookhaven National Laboratory (reference: 3EBX, R3EBXSF).

localized on the concave side. It also shows that the side chains conserved in all the curaremimetic toxins have a similar global orientation in toxin α and erabutoxin b. These side chains may thus be essential for the binding to AcChoR, in agreement with previous proposals (Low et al., 1976; Karlsson et al., 1979; Endo & Tamiya, 1987). A more precise delineation of the toxic site is currently being investigated by site-directed mutagenesis of erabutoxin b, using the toxin expression system described previously (Ducancel et al., 1989; Boyot et al., 1990).

The coordinates of the eight converged structures of toxin α have been deposited in the Brookhaven Protein Data Bank. The complete list of experimental restraints and the figure representing the side-chain surface accessibilities of the X-PLOR structures are available from the authors.

## ACKNOWLEDGMENT

We thank K. Wüthrich for providing us with a copy of the DIANA program and A. Brünger for the copy of the X-PLOR program.

## REFERENCES

Agard, D. A., & Stroud, R. M. (1982) *Acta Crystallogr. A38*, 186–194.

Aue, W. P., Bartholi, E., & Ernst, R. R. (1976) *J. Chem. Phys. 64*, 2229–2246.

Basus, V. J., Billeter, M., Love, R. A., Stroud, R. M., & Kuntz, I. D. (1988) *Biochemistry 27*, 2763–2771.

Betzel, C., Lange, G., Pal, G. P., Wilson, K. S., Maelicke, A., & Saenger, W. (1991) *J. Biol. Chem. 266*, 21530–21536.

Bodenhausen, G., Kogler, H., & Ernst, R. R. (1984) *J. Magn. Reson. 58*, 370–388.

Bontems, F., Gilquin, B., Roumestand, C., Ménez, A., & Toma, F. (1992) *Biochemistry 31*, 7756–7764.

Bourne, P. E., Sato, A., Corfield, P. W. R., Rosen, L. S., Birken, S., & Low, B. W. (1985) *Eur. J. Biochem. 153*, 521–527.

Boyot, P., Pillet, L., Ducancel, F., Boulain, J.-C., Trémeau, O., & Ménez, A. (1990) *FEBS Lett. 266*, 87–90.

Brooks, B. R., Bruccoleri, R. E., Olafson, B. D., States, D. J., Swaminathan, S., & Karplus, M, (1983) *J. Comput. Chem. 4*, 187–217.

Brünger, A. T. (1988) *X-PLOR Manual*, The Howard Hughes Medical Institut and Departement of Molecular Biophysics and Biochemistry, Yale University, New Haven, CT.

Brünger, A. T., Kuriyan, K., & Karplus, M. (1987) *Science 235*, 458–460.

Bystrov, V. F., Tsetlin, V. I., Karlsson, E., Pashkov, V. S., Utkin, Y., Kondakov, V. I., Pluzhnikov, K. A., Arseniev, A. S., Ivanov, V. T., & Ovchinnikov, Y. A. (1983) in *Toxins as Tools in Neurochemistry* (Hucho, F., & Ovchinnikov, Y. A., Eds.) pp 193–233, Walter de Gruyter, Berlin.

Clore, G. M., & Gronenborn, A. M. (1991) *J. Mol. Biol. 220*, 47–53.

Clore, G. M., Gronenborn, A. M., Nilges, M., & Ryan, C. A. (1987) *Biochemistry 26*, 8012–8023.

Clore, G. M., Appela, E., Yamada, M., Matsushima, K., & Gronenborn, A. M. (1990) *Biochemistry 29*, 1689–1696.

Corfield, P. W. R., Lee, T.-J., & Low, B. W. (1989) *J. Biol. Chem. 264*, 9239–9242.

Davis, D. G., & Bax, A. (1985) *J. Am. Chem. Soc. 107*, 2820–2821.

Ducancel, F., Boulain, J.-C., Trémeau, O., & Ménez, A. (1989) *Protein Eng. 3*, 139–143.

Dufton, M. J., & Hider, R. C. (1977) *J. Mol. Biol. 115*, 177–193.

Dufton, M. J., & Hider, R. C. (1988) *Pharmacol. Ther. 36*, 1–40.

Eaker, D., & Porath, J. (1967) *Proc. Plenary Sess., Int. Congr. Biochem., 7th, 1967 (1968)*, Col. VIII-3, Abstr. III, p 499.

Endo, T., & Tamiya, N. (1987) *Pharmacol. Ther. 34*, 403–451.

Faure, G., Boulain, J.-C., Bouet, F., Montenay-Garestier, Th., Fromageot, P., & Ménez, A. (1983) *Biochemistry 22*, 2068–2076.

Fryklund, L., & Eaker, D. (1975) *Biochemistry 14*, 2865–2871.

Gippert, G. P., Yip, P. F., Wright, P. E., & Case, D. A. (1990) *Biochem. Pharmacol. 40*, 15–22.

Güntert, P., Braun, W., & Wüthrich, K. (1991) *J. Mol. Biol. 217*, 517–530.

Hider, R. C., Drake, A. F., Inagaki, F., Williams, R. J. P., Endo, T., & Miyazawa, T. (1982) *J. Mol. Biol. 158*, 275–291.

Inagaki, F., Hider, R. C., Hodges, S. J., & Drakes, A. F. (1985) *J. Mol. Biol. 183*, 575–590.

Karlsson, E. (1979) in *Handbook of Experimental Pharmacology* (Lee, C.-Y., Ed.) Vol. 52, pp 159–212, Springer-Verlag, Berlin.

Kondakov, V. I., Arseniev, A. S., Plushnikov, K. A., Tsetlin, V. I., Bystrov, V. F., & Ivanov, V. T. (1984) *Bioorg. Khim. 10*, 1606–1628.

Kraulis, P. J., Clore, G. M., Nilges, M., Jones, T. A., Petterson, G., Knowles, J., & Gronenborn, A. M. (1989) *Biochemistry 28*, 7241–7257.

Kumar, A., Ernst, R. R., & Wüthrich, K. (1980) *Biochem. Biophys. Res. Commun. 64*, 2229–2246.

Labhardt, A. M., Hunziker-Kwik, E.-M., & Wüthrich, K. (1988) *Eur. J. Biochem. 177*, 295–305.

LaPlante, S. R., Mikou, A., Robin, M., Guittet, E., Delsuc, M.-A., Charpentier, I., & Lallemand, J.-Y. (1990) *Int. J. Pept. Protein Res. 36*, 227–230.

Le Goas, R., LaPlante, S. R., Mikou, A., Delsuc, M.-A., Guittet, E., Robin, M., Charpentier, I., & Lallemand, J.-Y. (1992) *Biochemistry 31*, 4867–4875.

Love, R. A., & Stroud, R. M. (1986) *Protein Eng. 1*, 37–46.

Low, B. W., & Corfield, P. W. R. (1986) *Eur. J. Biochem. 161*, 579–587.

Low, B. W., Preston, H. S., Sato, A., Rosen, L. S., Searl, J. E., Rudko, A. D., & Richardson, J. S. (1976) *Proc. Natl. Acad. Sci. U.S.A. 73*, 2991–2994.

Ménez, A., Bouet, F., Tamiya, N., & Fromageot, P. (1976) *Biochim. Biophys. Acta 453*, 121–132.
Ménez, A., Langlet, G., Tamiya, N., & Fromageot, P. (1978) *Biochimie 60*, 505–516.
Ménez, A., Montenay-Garestier, T., Fromageot, P., & Hélène, C. (1980) *Biochemistry 19*, 5202–5208.
Ménez, A., Boulain, J.-C., Faure, G., Couderc, J., Liacopoulos, P., Tamiya, N., & Fromageot, P. (1982) *Toxicon 20*, 95–103.
Ménez, A., Tamiya, T., Guignery-Frelat, G., Bouet, F., Mallet, J., Boulain, J.-C., & Fromageot, P. (1986) *Pure Appl. Chem. 58*, 407–414.
Ménez, A., Pillet, L., Léonetti, M., Bontems, F., & Maillère, B. (1991) Snake toxins as antigens, in *Structure of Antigens* (Van Regenmortel, Ed.) Chapter 13, Telford Press, London.
Meunier, J.-C., Olsen, R. W., Ménez, A., Fromageot, P., Boquet, P., & Changeux, J.-P. (1972) *Biochemistry 11*, 1200–1210.
Nilges, M., Clore, G. M., & Gronenborn, A. M. (1988) *FEBS Lett. 229*, 317–324.
Omichinski, J., Clore, G. M., Appella, E., Sakaguchi, K., & Gronenborn, A. M. (1990) *Biochemistry 29*, 9324–9334.
Popot, J.-L., & Changeux, J.-P. (1984) *Physiol. Rev. 64*, 1162–1239.
Rance, M., Sørensen, O., Bodenhausen, G., Wagner, G., Ernst, R. R., & Wüthrich, K. (1983) *Biochem. Biophys. Res. Commun. 117*, 479–485.
Richardson, J. (1981) *Adv. Protein Chem. 34*, 167–330.
Smith, J. L., Corfield, P. W. R., Hendrickson, W. A., & Low, B. W. (1988) *Acta Crystallogr. A44*, 357–368.
Tsernoglou, D., & Petsko, G. A. (1976) *FEBS Lett. 68*, 1–4.
Wagner, G., & Zuiderweg, E. R. P. (1983) *Biochem. Biophys. Res. Commun. 113*, 854–860.
Wagner, G., Braun, W., Havel, T. F., Schaumann, T., Go, N., & Wüthrich, K. (1987) *J. Mol. Biol. 196*, 611–639.
Walkinshaw, M. D., Säenger, W., & Maelicke, A. (1980) *Proc. Natl. Acad. Sci. U.S.A. 77*, 2400–2404.
Weber, M., & Changeux, J.-P. (1974) *Mol. Pharmacol. 10*, 1–14.
Wüthrich, K. (1976) *NMR in Biological Research: Peptides and Proteins*, North Holland, Amsterdam.
Wüthrich, K. (1986) *NMR of Proteins and Nucleic Acids*, Wiley-Interscience Publication, New York.
Wüthrich, K., Billeter, M., & Braun, W. (1983) *J. Mol. Biol. 169*, 949–961.
Yu, C., Lee, C.-S., Chuang, L.-C., Shei, Y.-R., & Wang, C. Y. (1990) *Eur. J. Biochem. 193*, 789–799.

**Registry No.** Erabutoxin b, 9083-23-2.